

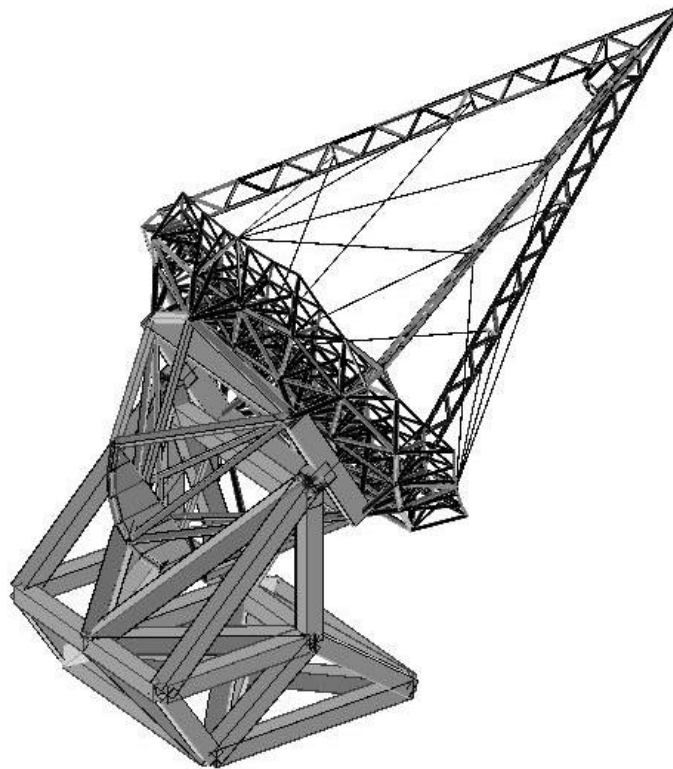
APPENDIX 5.5.A

IMPLICATIONS OF THE NOBEYAMA WIND TESTING RESULTS FOR THE GSMT

Paper written for the New Initiatives Office, November 2001.



IMPLICATIONS OF THE NOBEYAMA WIND TESTING RESULTS FOR THE GMST



DAVID SMITH

MERLAB, PC

Mechanical Engineering Research Laboratory, 309 S. McDonough St., Decatur, GA 30030-3719

Table of Contents

1. SUMMARY	3
2. INTRODUCTION	3
3. OCTOBER 1999 TESTS AT THE NRO 45m	4
3.1 Measurement Approach	4
3.3 Summary of Results	5
4. DEFORMATIONS OF THE PRIMARY	6
4.1 Parked Telescope, Calm Wind.....	6
4.2 Tracking Telescope, Calm Wind (<2m/s).....	7
4.3 Parked Telescope, Significant Wind (6-8 m/s)	8
5. DEFORMATIONS OF THE SECONDARY	8
5.1 Parked Telescope, Calm Wind (<2 m/s).....	8
5.2 Tracking Telescope, Calm Wind (<2 m/s)	9
5.3 Parked Telescope, Significant Wind (6-8 m/s).....	10
5.4 RMS Motions of the Secondary	10
6. CONCLUSIONS	12

IMPLICATIONS OF THE NOBEYAMA WIND TESTING RESULTS FOR THE GMST

1. SUMMARY

In order to quantify the wind-induced dynamic pointing errors on a large radio telescope, a series of experiments was conducted using the Nobeyama Radio Observatory (NRO) 45m telescope. These tests provided information on both the on-sky pointing of the antenna and the physical motions of the structure.

While the original purpose of the test was to investigate dynamic pointing variations, the data are relevant and useful to the design of the GSMT. The data provide direct measurement of the typical amplitude and frequency content of structural motions on a large reflector truss as well as on the secondary (M2) support. Additionally, the natural frequency of the structure is in the same range as that expected for GSMT.

The results show that the dynamic surface errors on the GSMT are likely to be several microns on the primary (M1) and that motions of tens of microns are likely at M2. To reduce these values to the level correctable by the downstream AO system ($\sim 1\mu\text{m}$), the M1 figure errors must be corrected to about 4 Hz and the M2 support must be stabilized to about 3-4 Hz.

2. INTRODUCTION

Wind-induced structural distortion is perhaps the most difficult challenge facing the designers of extremely large optical/IR telescopes. Such deformations are important not only at M1, where they affect the surface figure, but also at M2, where they cause rigid body motions. Unlike gravity and thermally-induced effects, the deformations due to wind loads are neither repeatable nor slowly varying. Thus, they can change quickly and cannot be removed by a lookup table. As an additional complication for large structures, the frequency content of the wind has the potential to affect the dynamics of the telescope, resulting in deformations much greater than expected from the static stiffness.

Even with a high-fidelity numerical model of a telescope, it is difficult to predict its dynamic response. Specifically, the spectrum of the wind is not well known, and its interaction with a complex structure is even more uncertain. As a result, obtaining good predictive results from a model is very challenging, and may even be impossible without a validation experiment. Such experiments cannot be scaled easily to wind tunnel testing, as the frequency response of a structure does not scale the same way as the bulk model scaling.

To assist in the understanding of this problem, we can make use of a series of structural and pointing measurements taken at the NRO 45m telescope in October 1999. These measurements include astronomical observations combined with simultaneous accelerometer measurements. In total, there are nine nights of observing data and five days/nights of structural data. The observing data consists primarily of 100 GHz continuum measurements on the limb of the Moon, with a few scans on Saturn and Jupiter. The structural data includes 44 channels of accelerometer data, together with some monitoring of other system information. The Modal Analysis and Controls Laboratory (MACL) at UMass Lowell, together with the vibrations laboratory from Michigan Technological University, conducted the tests, using both their own equipment and other equipment loaned for the purpose by PCB Piezotronics and The Modal Shop, Inc. These tests were originally performed in order to answer questions related to pointing errors of a large radio telescope. However, because of the type and distribution of sensors used in the tests, these tests contain information which is useful to the GSMT design.

3. OCTOBER 1999 TESTS AT THE NRO 45M

3.1 MEASUREMENT APPROACH

The October 1999 observation run combined astronomical pointing measurements with simultaneous multi-channel measurements of the behavior of the structure. As a result, the tests measured the on-sky pointing error and the structural motions simultaneously. For purposes of the GSMT design, the relevant data are the structural results.

The structural measurements were made under a variety of conditions. These included static tests, tracking tests, slewing tests, and simultaneous measurements during observations.

The static tests consisted of a passive structural characterization of the antenna at a variety of elevation angles. This provided a demonstration of the typical variation in response frequencies and operating shapes of a large antenna as it moves in elevation. Additionally, these results provided a baseline response for comparison. While this data set could be combined with an FE model to extract the forcing function on the structure, such an approach is limited by the lack of a calibrated modal test.

The tests were then repeated while the antenna was tracking a sidereal-rate source. This was performed to reveal any controller-induced variations in the performance.

The third series of tests were taken while slewing the antenna in order to obtain information about ring-down time and overshoot. These tests are not relevant to the observational performance of the system, and are not covered here.

Finally, the integrated pointing tests were performed. In these tests, we tracked on the limb of the Moon and monitored the continuum signal while subtracting out the sky. Calibration of the data was performed by measuring a known load and by taking constant-rate scans across the target. While taking the astronomical data, the acquisition system recorded data from the accelerometers, as well as from a few voltage signals available at the antenna. These extra signals included a clock pulse to enable synchronization of the data, and a direct monitor of the receiver pixel #1 output.

3.2 HARDWARE

The astronomical data were obtained with the Nobeyama S-115Q 4-pixel SiS receiver, operating in continuum mode at 100 GHz. The structural data were obtained using high-sensitivity, low-frequency accelerometers. Two types of accelerometers were used in the experiment. The first were DC accelerometers which had been modified to reduce their noise (resulting in a floor of around $50\mu\text{g}'\text{s}$). The second were the larger seismic accelerometers, which have a noise of about $5\mu\text{g}'\text{s}$. These were arranged on the structure as follows (see Figure 1):

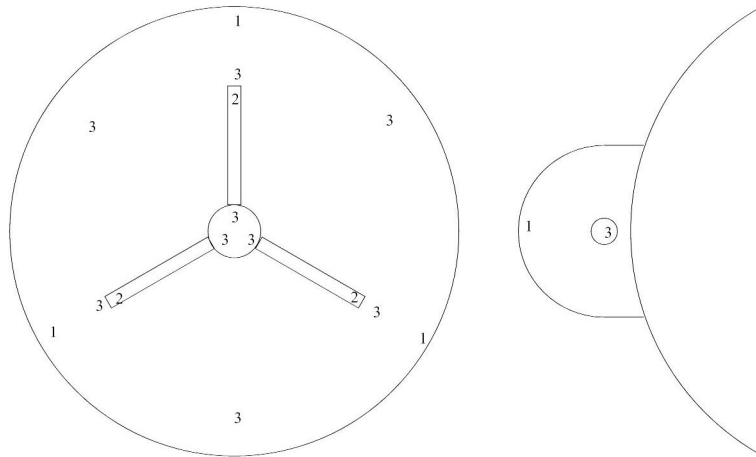


Figure 1: Location and Number of Accelerometers

Primary reflector:

21 sensors (18 seismic arranged as 6 triaxes, and 3 DC)

Secondary reflector:

9 sensors arranged as 3 triaxes: 6 seismic, 3 of DC

Secondary support tripod:

6 sensors (two DC accels at the base of each leg)

Elevation axis:

6 sensors (seismic accelerometers arranged as a triax on each end of the axis)

Elevation drive arcs:

2 sensors (1 DC accel measuring tangentially on each arc)

The position resolution of the seismic accelerometers is about $1\mu\text{m}$ amplitude at 1 Hz, and improves with the square of the frequency. Other information about the system was also monitored, and is listed below:

- Channel 1 of astronomy data
- Minute Clock
- Azimuth tachometers (last two nights)
- Azimuth current feedback monitor (last two nights)

3.3 SUMMARY OF RESULTS

The data from the October run is extensive, but much of the useful information can be illustrated with a few typical cases. In the sections below, we examine the response of a typical accelerometer on the primary reflector and a triaxial accelerometer at the secondary. In each case, the power spectral density (PSD) is presented, together with a plot of the total RMS motion of the accelerometer at and above each frequency. The latter plot serves to illustrate the minimum frequency correction necessary to provide a residual below a given specification (set,

for example, by downstream AO capabilities). For each case, the results are presented for three different test conditions:

1. Parked Telescope, Calm Wind (<2m/s)
2. Tracking Telescope, Calm Wind (<2m/s)
3. Parked Telescope, Significant Wind (6-8m/s)

4. DEFORMATIONS OF THE PRIMARY

In considering the deformation of a typical point on the primary, it is important to note that much of the signal may be due to a rigid body tilt of the reflector. While this is important to the pointing performance, it does not affect the RMS surface quality. To address this, the PSD's below are shown for both the raw signal and for the signal after removal of the best fit plane of all of the accelerometers on M1. In all cases, the figures show the output of the seismic accelerometer oriented normal to the surface and located near the base of the M2 support leg in the 12 o'clock position (see Figure 1). All figures are shown on the same axis scale to aid visual comparison. In calm conditions, there is little difference between the spectra. However, in tracking or windy conditions, the signal is dominated (except at a few frequencies) by the rigid body signal. In the generation of the plots of RMS at/above a given frequency, these rigid body motions have been removed.

4.1 PARKED TELESCOPE, CALM WIND

As shown in Figure 2, under maximally calm conditions the ambient vibration response of the primary reflector is low. Further, it is essentially a broadband response that is uncorrelated with a tilt of the reflector. This is demonstrated by the similarity between the raw trace and the trace with the best-fit plane removed. Examining the structural RMS implied by this result (lowest trace in Figure 3), we see that the response is dominated by sensor noise to about 1 Hz, where an ambient vibration of $\sim 1\mu\text{m}$ is present.

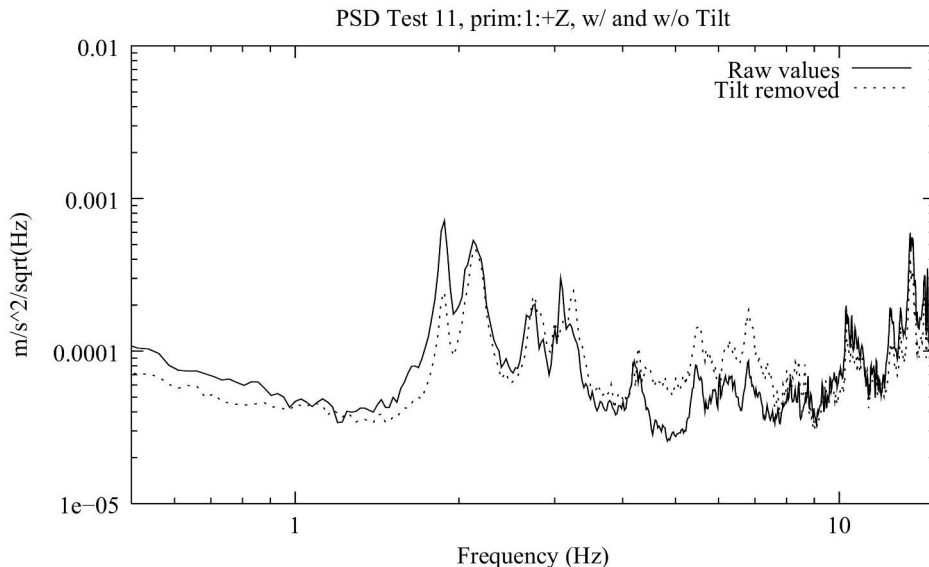


Figure 2: Parked Telescope, Calm Wind

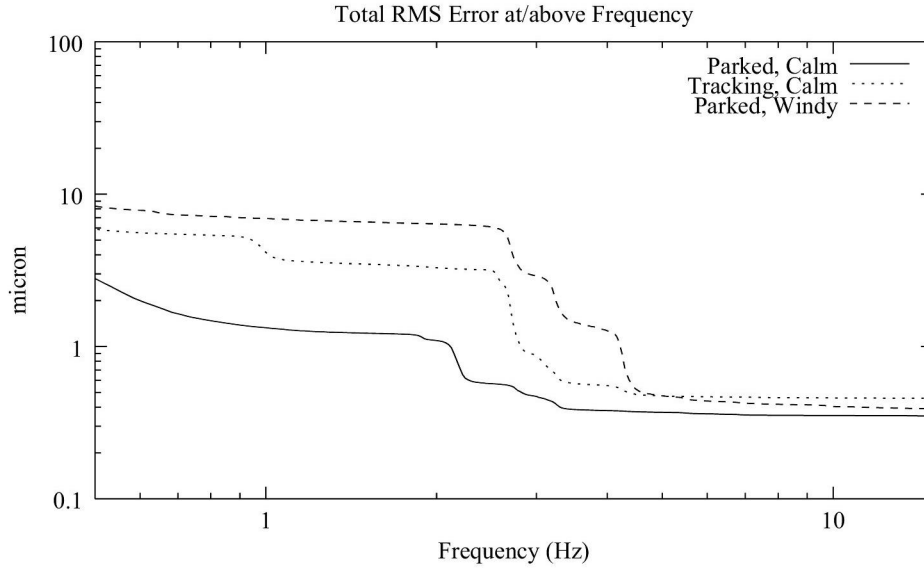


Figure 3: RMS Comparison (all cases)

4.2 TRACKING TELESCOPE, CALM WIND (<2M/S)

Figure 4 shows the structural response of the same portion of the telescope during tracking of the Moon. The resulting spectrum is about an order of magnitude higher than the first case, but most of this is due to rigid body tilts of the reflector. Examination of the RMS (Figure 3) implies that, even with the removal of these tilts, telescope tracking introduces about $5\mu\text{m}$ of broadband vibration disturbance into the structure. Similarly, it is not until around 2.5 Hz that the response drops below the $1\mu\text{m}$ level. It is worth noting that the substantial peak at ~ 0.9 Hz has been traced to the controller and corrected. Additionally, the NRO 45m is a wheel-on-track telescope, and the hydrostatic bearings used by many large optical telescopes may well reduce some of this effect.

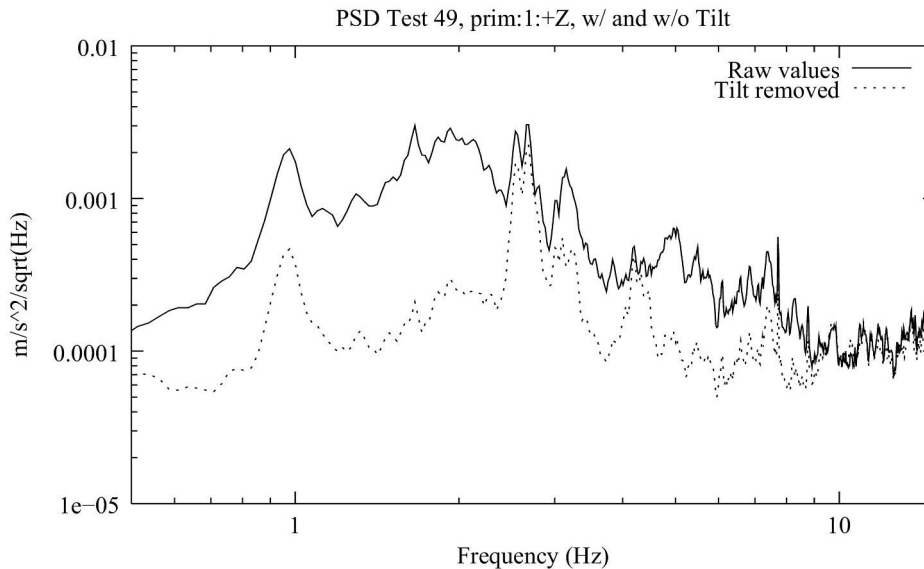


Figure 4: Tracking Telescope, Calm Wind

4.3 PARKED TELESCOPE, SIGNIFICANT WIND (6-8 M/S)

As would be expected, the presence of significant wind loading on the telescope adds to the overall response of the structure (Figure 5). Indeed, for these conditions, the responses were on the order of the same value as the telescope tracking tests. However, in this case, certain distinct frequency peaks are clearly excited (because they are structural modes or, possibly, because of interaction with the of wind around the structure). At these peaks, removal of the best-fit plane from the data has no appreciable effect on the response. Because of the strong excitation of these peaks, the windy conditions produce the largest structural RMS, which is above $8\mu\text{m}$ below 1 Hz, and which does not drop to below $1\mu\text{m}$ until above 4 Hz.

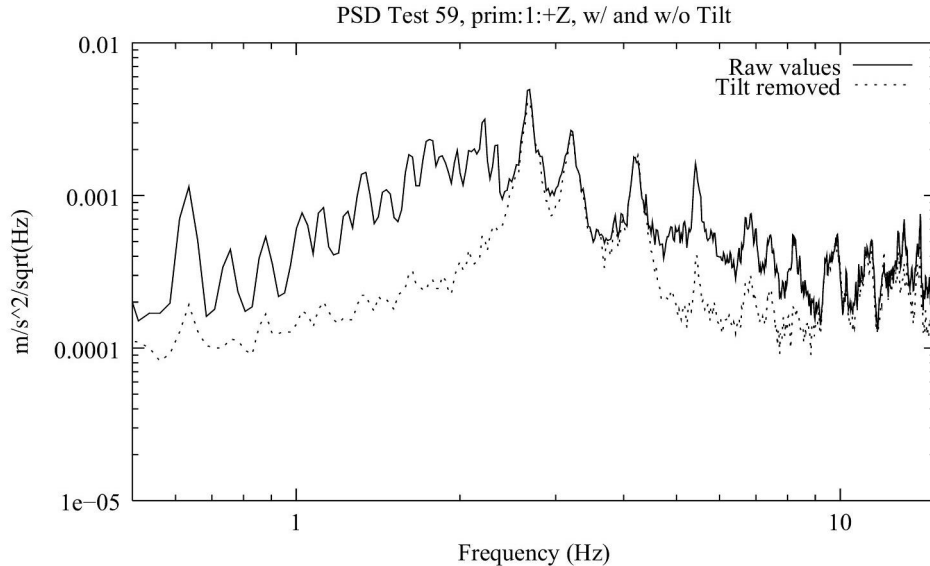


Figure 5: Parked Telescope, Wind 6-8 m/s

5. DEFORMATIONS OF THE SECONDARY

Any measured motion of the secondary reflector may be due to the overall rigid body motion of the structure, or it may be due to deflections with respect to that rigid body position. Since the NRO 45m secondary support structure is independent of the primary reflector truss, however, we can only use the raw values in analyzing the signal. That is, some component of the results shown below would not cause any aberrations because it would arise out of the rigid body tilt of a perfectly aligned telescope. It is also worth noting that some failed channels in the experiment prevent extraction of the tip and tilt of the secondary, so the measurements shown below may also be confounded with local tip/tilt effects. However, these results still provide a useful indicator of the scale of the motions of M2.

In all of the cases shown below, the `X' direction is directed along the circumference of M2, `Y' is the radial direction, and `Z' is along the boresight of the telescope. Generally, `Y' and `Z' have similar amplitudes and frequency responses while `X' is smaller and of qualitatively different behavior. The difference between `X' and `Y' suggests that the dominant behavior is a tilt of M2 rather than a decentering.

5.1 PARKED TELESCOPE, CALM WIND (<2 M/S)

As shown in Figure 6, under maximally calm conditions the ambient vibration response of the secondary reflector is low. There is some evidence of the first few telescope modes, followed by

what appear to be local vibrational responses. There is also a peak in the 6-7 Hz range that is characteristic of the M2 support response for this telescope.

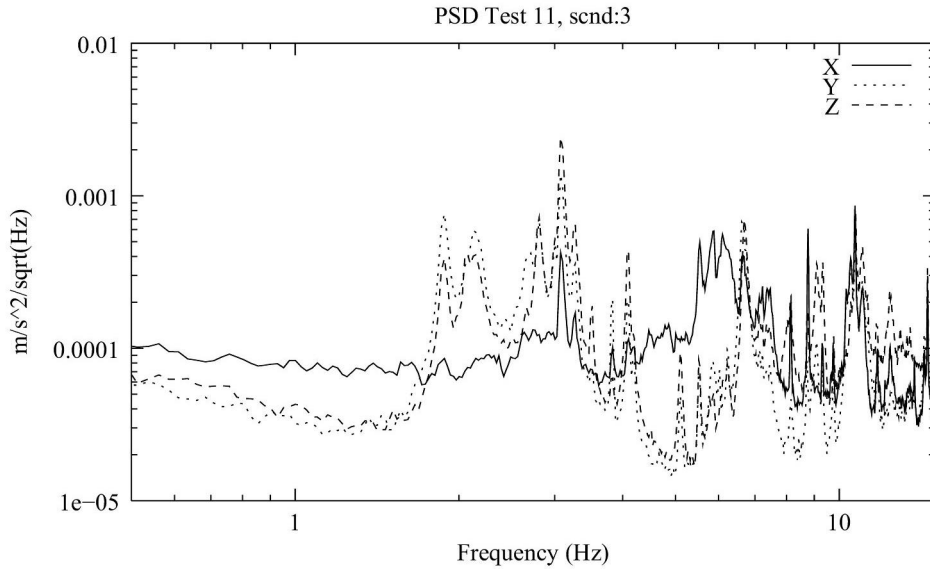


Figure 6: Parked Telescope, Calm Wind

5.2 TRACKING TELESCOPE, CALM WIND (<2 M/S)

As with the primary, the response at the secondary reflector increases dramatically when the telescope begins to track (Figure 7). This response is almost certainly dominated by rigid body motions, as the shape of the response is quite similar to that seen at the primary in the raw signal (including the presence of the peak at ~0.9 Hz).

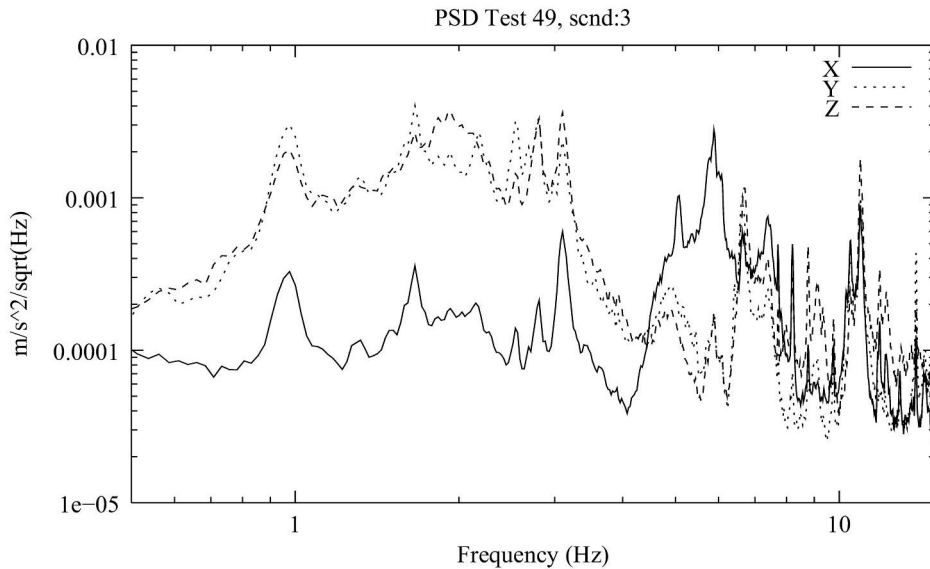


Figure 7: Tracking Telescope, Calm Wind

5.3 PARKED TELESCOPE, SIGNIFICANT WIND (6-8 M/S)

As in the previous case, the response (at least in the 'Y' and 'Z' directions) is qualitatively similar to the response at the primary, suggesting that this is largely a rigid body response. The strong peaks in the 6-7 Hz region are also still present, however (Figure 8).

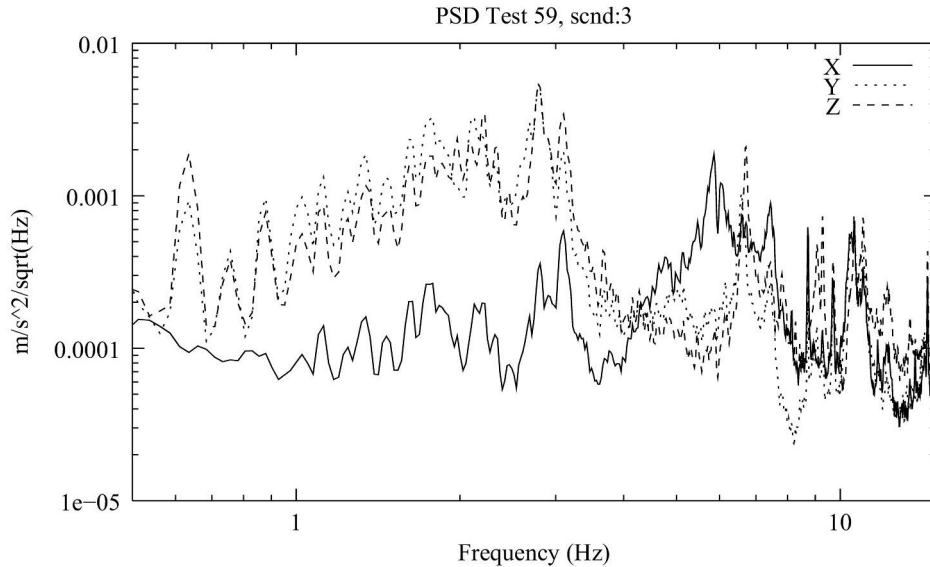


Figure 8: Parked Telescope, Wind 6-8 m/s

5.4 RMS MOTIONS OF THE SECONDARY

The structural RMS implied by the PSD's of the secondary motions is shown in Figures 9-11. In the 'X' direction, it can be seen that the response is dominated by sensor noise to about 1-2 Hz, where an ambient vibration of a few microns is present. This remains constant to about 6 or 7 Hz (the major secondary support mode); above that the amplitudes drop substantially. Even in the windy case, the RMS is only on the order of 2-3 μ m for frequencies above 1 Hz.

In the 'Y' and 'Z' directions, the response is much higher, with low frequency RMS of tens of microns under tracking or windy conditions. However, the response falls off sharply (to below 1 μ m) above the first few modes of the telescope (~ 3 Hz). This suggests that the motions are largely due to the complete structure rather than independent deformations of the secondary support.

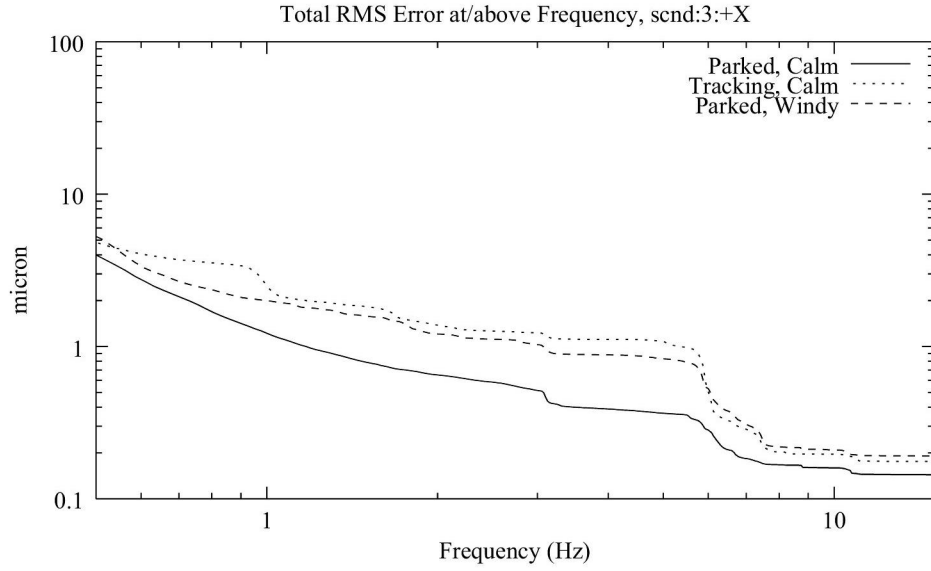


Figure 9: RMS Comparison, X-direction

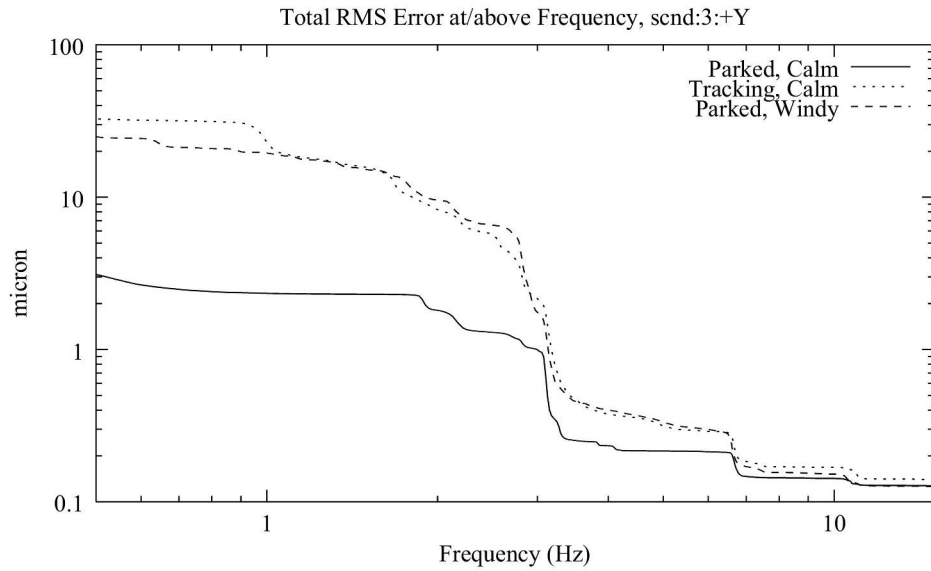


Figure 10: RMS Comparison, Y-direction

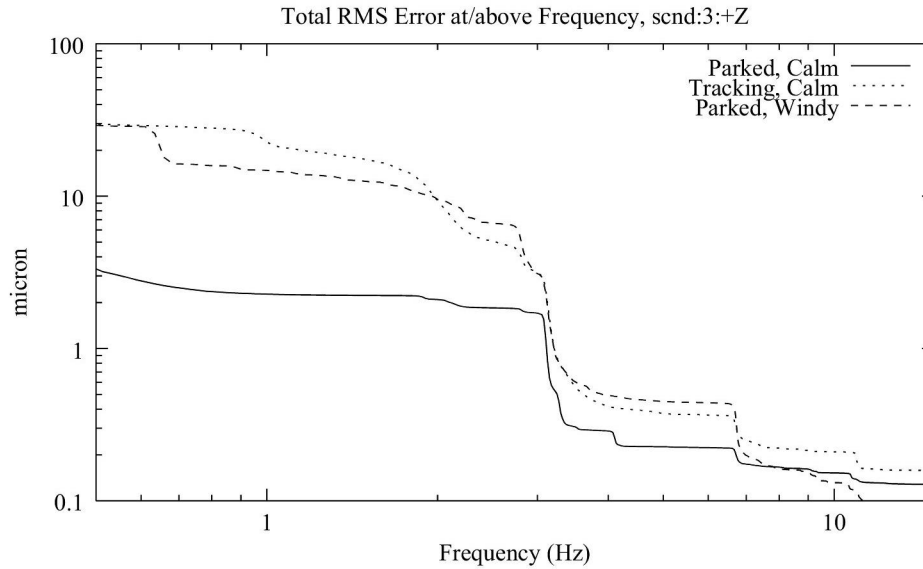


Figure 11: RMS Comparison, Z-direction

6. CONCLUSIONS

From the NRO 45m data, we can see that a large, unenclosed structure can be vibrationally quiet to about $1\mu\text{m}$ RMS under exceptionally calm conditions. However, vibrations due to either telescope tracking motions or external wind loads can be an order of magnitude higher. To reduce these errors to the $1\mu\text{m}$ RMS level, it would be necessary to correct for M1 surface errors at about 4 Hz and M2 motions at about 3-4 Hz.

Aside from the information on the necessary control system bandwidth for eliminating these errors, there are some other useful lessons from this data set. While these lessons do not place new constraints on the GSMT design, the data presented here place an order of magnitude on the effects and confirm their importance. The first of these is that the mechanical vibrations introduced just by driving the telescope can be substantial over a wide frequency range. This confirms that the GSMT design must address this in the mechanical design of the drive systems as well as in the motion planning and control software. It also appears that special attention may be necessary in the design of the enclosure ventilation and rotation systems to make sure that such external mechanical vibrations do not degrade performance. Finally, the magnitude of the wind response, even out to several Hz, indicates that the typical wind speed at the site and the availability of a wind-protecting enclosure will have a substantial impact on the available observing conditions.

The New Initiatives Office is a partnership between two divisions of the Association of Universities for Research in Astronomy (AURA), Inc.: the National Optical Astronomy Observatory (NOAO) and the Gemini Observatory.

NOAO is operated by AURA under cooperative agreement with the National Science Foundation (NSF).

The Gemini Observatory is operated by AURA under a cooperative agreement with the NSF on behalf of the Gemini partnership: the National Science Foundation (United States), the Particle Physics and Astronomy Research Council (United Kingdom), the National Research Council (Canada), CONICYT (Chile), the Australian Research Council (Australia), CNPq (Brazil) and CONICET (Argentina).